J Biol Inorg Chem (2014) 19:449–464
DOI 10.1007/s00775-014-1089-6

ORIGINAL PAPER

Synthesis, characterization, and binding properties towards CT-DNA and lipoxygenase of mixed-ligand silver(I) complexes with 2-mercaptothiazole and its derivatives and triphenylphosphine

L. Kyros · C. N. Banti · N. Kourkoumelis · M. Kubicki · I. Sainis · S. K. Hadjikakou

Received: 19 August 2013 / Accepted: 29 December 2013 / Published online: 21 January 2014

Abstract Mixed-ligand silver(I) complexes of formulae $[AgCl(TPP)_2(MTZD)]$ (**1**), $\{[AgCl(TPP)_2(MBZT)]\cdot(MBZT)\cdot 2(toluene)\}$ (**2**), and $[AgCl(TPP)_2(CMBZT)]$ (**3**) were obtained by refluxing toluene solutions of silver(I) chloride with triphenylphosphine (TPP) and the appropriate heterocyclic thioamides 2-mercaptothiazolidine (MTZD), 2-mercaptobenzothiazole (MBZT), and 5-chloro-2-mercaptobenzothiazole (CMBZT). The complexes were characterized by the melting point, vibrational spectroscopy (Fourier transform mid-IR), ^{1}H-NMR spectroscopy, UV–vis spectroscopy, and X-ray crystallography. DNA binding tests indicate the ability of complexes **1**–**3** to modify the activity of cells. The binding constants of **1**–**3** towards calf-thymus DNA (CT-DNA) [$(3.5 \pm 8.5) \times 10^4$ M^{-1} for **1**, $(10.0 \pm 0.0) \times 10^4$ M^{-1} for **2**, and $(46.4 \pm 7.0) \times 10^4$ M^{-1} for **3**] indicate strong interaction of **3**. Changes in the fluorescence of ethidium bromide in the presence of DNA suggest intercalation into or electrostatic interactions with DNA. The corresponding apparent binding constants (K_{app}) towards CT-DNA calculated through fluorescence spectra are $(3.5 \pm 0.7) \times 10^4$ M^{-1} for **1**, $(10.0 \pm 0.0) \times 10^4$ M^{-1} for **2**, and $(46.4 \pm 7.0) \times 10^4$ M^{-1} for **3**. Docking studies on DNA complexes confirm the binding of **1** and **2** in the major groove of CT-DNA and of **3** in the minor groove. Moreover, the influence of **1**–**3** on the catalytic peroxidation of linoleic acid to hydroperoxylinoleic acid by the enzyme lipoxygenase was studied kinetically and theoretically. The antibacterial effect of **1**–**3** against the bacterial species *Pseudomonas aeruginosa* and *Escherichia coli* was evaluated. Complex **1** exhibits the strongest activity.

Keywords Bioinorganic chemistry · Silver(I) chloride complexes · Heterocyclic thioamides · DNA binding · Antibacterial activity

An interactive 3D complement page in Proteopedia is available at: http://proteopedia.org/w/Journal:JBIC:25.

Electronic supplementary material The online version of this article (doi:10.1007/s00775-014-1089-6) contains supplementary material, which is available to authorized users.

L. Kyros · C. N. Banti · S. K. Hadjikakou (✉)
Section of Inorganic and Analytical Chemistry,
Department of Chemistry,
University of Ioannina,
45110 Ioannina, Greece
e-mail: shadjika@uoi.gr

N. Kourkoumelis
Medical Physics Laboratory,
Medical School,
University of Ioannina,
45110 Ioannina, Greece

M. Kubicki
Department of Chemistry,
Adam Mickiewicz University,
Umultowska 89b,
61-614 Poznań, Poland

I. Sainis
Cancer Biobank Center,
University of Ioannina,
45110 Ioannina, Greece

Introduction

Silver has been recognized as an effective antimicrobial agent, specifically in the form of silver nitrate, since the seventeenth and eighteenth centuries [1]. It has also been used in the treatment of chronic skin ulcers, open wounds, and suppurating wounds [2]. Nowadays, silver sulfadiazine

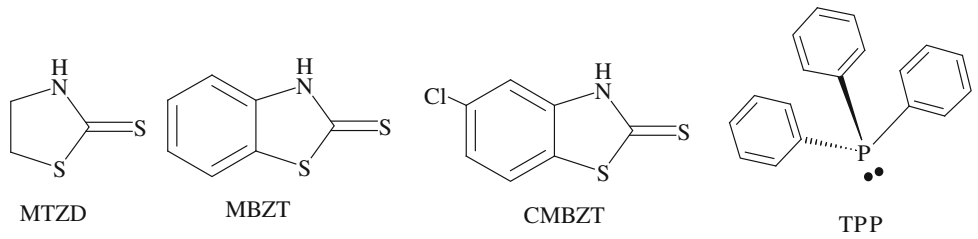

Structure 1

remains one of the most effective and widely used topical burn treatments [3, 4]. The astringent properties of silver against a wide range of bacteria have been recognized, and although the cytotoxic effects of silver against Gram-positive and Gram-negative bacteria have long been established, the exact mechanisms of action are not completely understood [1]. It has been reported that silver-treated bacterial cells exhibited a region in their cytoplasm with condensed DNA molecules [5]. Condensed DNA molecules lose their ability to replicate. Another mechanism was proposed, suggesting that the silver moiety in silver sulfadiazine is dissociated from sulfadiazine and binds to components within the cell. The subsequent inhibition of bacterial growth is due to the amount of silver bound to bacterial DNA [6]. Recently, the antitumor activity of silver(I) ions has been attributed to their interaction with nucleic acids, preferentially with the bases in DNA rather than with the phosphate groups [7].

We have recently shown that silver(I) complexes of the anti-inflammatory drugs salicylic acid ($salH_2$), aspirin (aspH), and naproxen (naprH) of formulae $[Ag(TPP)_2(salH)]$, $\{[Ag(TPP)_3(asp)](DMF)\}$, $\{[Ag(TPP)_3(napr)](H_2O)\}$, and $[Ag(TPTP)_2(napr)]$ [where TPP is triphenylphosphine, DMF is dimethylformamide, and TPTP is tri(*p*-tolyl)phosphine] interfere strongly with both calf-thymus DNA (CT-DNA) and lipoxygenase (LOX), leading to cell death through apoptosis [8, 9]. The binding affinity of the mixed-ligand silver(I) complex $[AgI(TPP)_2(MBZT)]$ (MBZT is 2-mercaptobenzothiazole) towards CT-DNA is minimal and towards LOX is negligible, causing mild cytotoxicity [10]. However, this complex does not interact with glutathione, which is responsible for the deactivation of cisplatin and for the development of the cells's resistance during chemotherapy, which makes the study of complexes of this type very interesting.

LOX is an enzyme that takes part in the metabolism of arachidonic acid. LOX catalyzes the oxidation of arachidonic acid to leukotrienes, in an essential mechanism for cell life [11, 12]. Prostaglandins, the final products formed from the metabolism of arachidonic acid, contribute to tumorigenesis as angiogenic factors [13]. Studies have shown that LOX inhibitors induce the release of cytochrome *c* from mitochondria into the cytosol, causing apoptosis through the mitochondrial pathway both in vivo and in vitro [14]. The literature data on bacterial LOXs are extremely limited, since these enzymes have only recently been found in prokaryotes (e.g., *Pseudomonas aeruginosa*) [15]. No bacterial LOXs have been detected in *Escherichia coli* [15]. A possible biological role of LOXs is to facilitate the dynamic plasticity of membranes in bacteria [15].

During our studies on the development of new metallotherapeutics [8–10, 16–30] which would be able to overcome the cell's resistance while still interacting with intracellular components and leading to cell death, we have synthesized novel silver(I) chloride complexes with TPP and the heterocyclic thioamides 2-mercaptothiazolidine (MTZD), MBZT, and 5-chloro-2-mercaptobenzothiazole (CMBZT) (Structure 1) of formulae $[AgCl(TPP)_2(MTZD)]$ (**1**), $\{[AgCl(TPP)_2(MBZT)]\cdot(MBZT)\cdot 2(toluene)\}$ (**2**), and $[AgCl(TPP)_2(CMBZT)]$ (**3**). The complexes were characterized by their melting point, vibrational spectroscopy (Fourier transform mid-IR), ^{1}H-NMR spectroscopy, UV–vis spectroscopy, and X-ray crystallography. Although the crystal structure of **1** is identical with the structure previously reported [31], we proceeded with its refinement once again for comparison with the structures of **2** and **3**. Moreover, the use of toluene instead of acetonitrile afforded **1** in 120 min and thus reduced the reaction time from 24 h. The binding affinity of **1**–**3** towards the intracellular molecules CT-DNA and LOX was studied for the evaluation of the mechanism of cell death. The ability to bind CT-DNA was tested by UV–vis, fluorescence, and docking studies. Kinetics and theoretical studies were used to investigate the influence of complexes **1**–**3** on the catalytic peroxidation of linoleic acid by the enzyme LOX. The antibacterial effect of **1**–**3** against the bacterial species *P. aeruginosa* and *E. coli* was also evaluated.

Results and discussion

General aspects

Complexes **1**–**3** were synthesized by refluxing for 2 h toluene solutions of silver(I) chloride, TPP, and the appropriate thioamide in a 1:2:1 molar ratio.

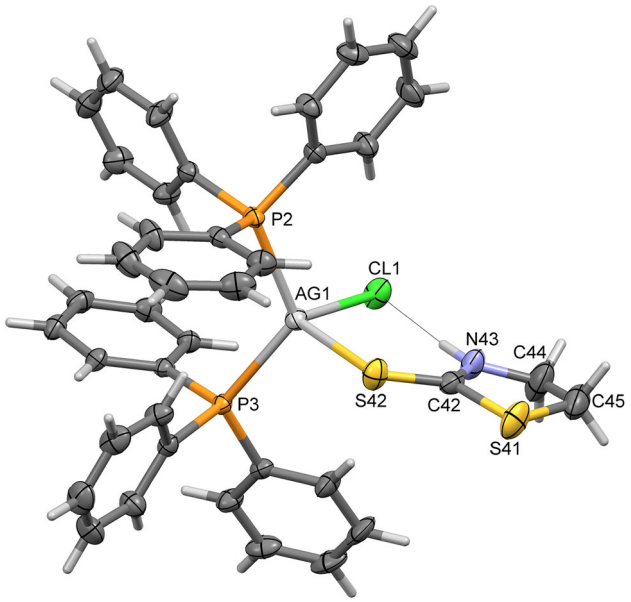

Fig. 1 Anisotropic ellipsoid diagram of $[AgCl(TPP)_2(MTZD)]$ (**1**), where TPP is triphenylphosphine and MTZD is 2-mercaptothiazolidine, together with the partial numbering scheme. The *ellipsoids* are drawn at the 33 % probability level. The intramolecular hydrogen bond is shown as a *dashed line*

$$AgCl + 2\,TPP + LS \xrightarrow[\text{reflux, 2 hrs}]{\text{toluene}} [AgCl(TPP)_2(LS)]$$

LS is MTZD (**1**), MBZT (**2**) and CMBZT (**3**).

Complex **1** was previously synthesized by heating, under reflux, the suspension which had been formed by silver(I) chloride and TPP in 1:2 ratio in acetonitrile for 24 h [31]. The white solid formed was then filtered off and was suspended in chloroform with MTZD in 1:1 silver-to-thione ratio. The suspension was stirred until a clear solution was obtained. Complex **1** was then recrystallized from dichloromethane from the solid that precipitated after evaporation of the solvent. However, here **1** is synthesized in high yield in one step. The full re-refinement of its structure was done for comparison with the structures of **2** and **3**, and the geometrical data are also required for the docking studies (see computational part). Crystals of complexes **1**–**3** are stable in air but were kept in darkness. Complexes **1**–**3** were soluble in toluene, acetonitrile, acetone, DMF, and dimethyl sulfoxide (DMSO).

Since dissociation of the Ag–P bonds might occur in solution [32], the stability of complexes **1**–**3** in DMSO solutions was tested by UV–vis spectra and ^{1}H-NMR spectra for 2 h as this is the duration of the biological experiments (interaction with DNA and LOX). No changes were observed between the initial UV and ^{1}H-NMR spectra and the corresponding spectra when measured after 2 h (Figs. S1, S2–S4). The stability of the complexes under UV light was also investigated. Irradiation of chloroform solutions of **1**–**3** with UV radiation at room temperature causes the gradual decomposition of the complex. Figure S5 shows the UV spectral changes in the region from 240 to 400 nm of a 2.5×10^{-5} M $CHCl_3$ solution of complexes **1**–**3** during irradiation (0–600 s) with UV light ($\lambda_{max} = 254$ nm) at room temperature using a low-pressure (15-W) mercury lamp (germicidal). A monotonic reduction of the absorbance is observed, with no appearance of new bands indicating photodecomposition of the complex. For the characterization of the photoproducts, a solution of 60 mg of complexes **1**–**3** in 10 ml chloroform was irradiated for 1 h in a quartz conical flask under aerobic conditions. The solutions were filtered and high-resolution mass spectra of the filtrates were recorded. The main species in these solutions are the $[Ph_3P{=}O]^+$ ion (**1**, **2**) and the $[Ph_3P{=}O{\bullet}Na]^+$ ion (**3**), indicating the decomposition of the initial complexes with formation of phosphine oxide, on irradiation of compounds **1**–**3** (Figs. S6–S8).

Vibrational spectroscopy

Thioamide vibrational bands I and II appear at 1,303–1,478 cm^{-1} (**1**) and 1,313–1,478 cm^{-1} (**2**, **3**) in the IR spectra of the complexes **1**–**3** (Figs. S7–S9), which are attributed to the ν(C=N) and ν(C–N) vibrations mainly undergoing a shift as compared with the corresponding vibrational bands of the free forms of the ligands, which are observed at 1,296–1,433 cm^{-1} (MTZD), 1,319–1,496 cm^{-1} (MBZT), and 1,312–1,453 cm^{-1} (CMBZT). Thioamide bands III and IV, attributed to the ν(C=S) and ν(C–S) vibrations, were observed at 697–1,050 cm^{-1} (MTZD), 751–1,035 cm^{-1} (MBZT), and 739–1,038 cm^{-1} (CMBZT) in the spectra of the free forms of the ligands and at 747–1,047 cm^{-1} (**1**), 744–1,025 cm^{-1} (**2**), and 745–1,022 cm^{-1} (**3**) in the spectra of complexes **1**–**3**. The band at 1,090 cm^{-1} in the IR spectra of **1**–**3** is assigned to the antisymmetric ν(C–P) vibrations and the bands at 507 cm^{-1} (**1**), 513 cm^{-1} (**2**), and 516 cm^{-1} (**3**) are assigned to the symmetric ν(C–P) vibrations of **1**–**3**. The corresponding ν(C–P) bands of the free form of the TPP ligand are observed at 1,088 cm^{-1} for the antisymmetric vibration and at 509 cm^{-1} for the symmetric vibration.

Crystal and molecular structures of **1**–**3**

Crystals of compounds **1**–**3** suitable for single-crystal X-ray analysis were grown by slow evaporation of the liquid remaining after filtration of the initial crops of solid material from the reactions of silver(I) chloride with the heterocyclic thioamides MTZD, MBZT, or CMBZT and TPP in a molar ratio of 1:1:2, respectively, in toluene. Although the crystal and molecular structures of compound

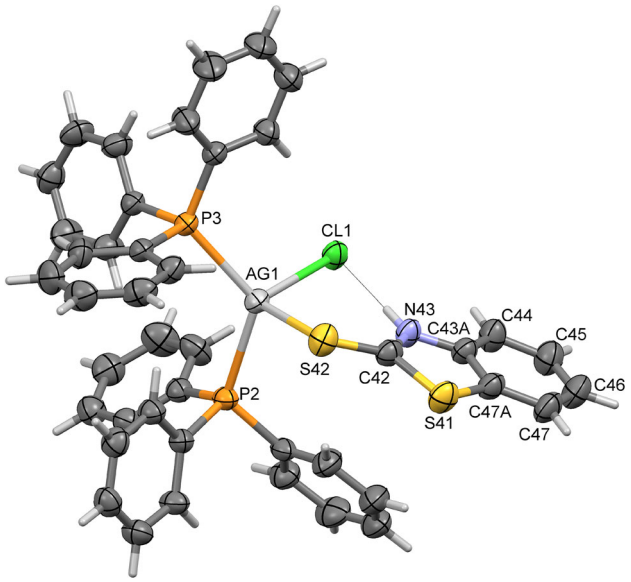

Fig. 2 Anisotropic ellipsoid diagram of {[AgCl(TPP)$_2$(MBZT)]·(MBZT)·2(toluene)} (**2**), where MBZT is 2-mercaptobenzothiazole, together with the partial numbering scheme. The *ellipsoids* are drawn at the 33 % probability level. The intramolecular hydrogen bond is shown as a *dashed line*. For clarity, other components of the crystal structure (free form of the ligand and solvent molecules) are not shown

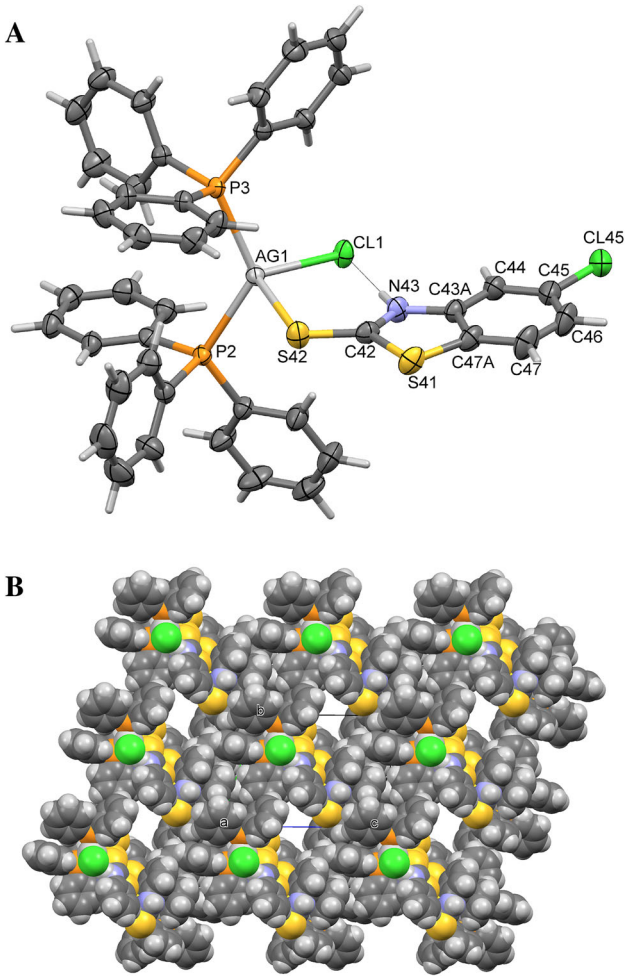

Fig. 3 **a** Anisotropic ellipsoid diagram of [AgCl(TPP)$_2$(CMBZT)] (**3**), where , and CMBZT is 5-chloro-2-mercaptobenzothiazole, together with the partial numbering scheme. The *ellipsoids* are drawn at the 33 % probability level. The intramolecular hydrogen bond is shown as a *dashed line*. **b** Packing of complex **2** after removal of the solvent molecules: the voids in the crystal structure are easily visible

1 were previously reported [31], we have reevaluated its structure here for comparison with the structures of **2** and **3**; its geometrical parameters were also used for the docking studies.

Figures 1, 2, and 3 show the displacement ellipsoid representations of complexes **1**–**3**.

In all three cases, the silver centers are four-coordinated—by two phosphorous atoms from TPP ligands, one sulfur atom from MBZT or CMBZT, and one chlorine atom, in a slightly distorted tetrahedral fashion; the distortion is mainly caused by the disposition of bulky TPP ligands. Table 1 lists the relevant geometrical parameters. In general, the Ag–P and Ag–Cl bond distances agree well with those found in similar structures (e.g., in [AgCl(TPP)$_2$(MTZD)] [31], [AgCl(TPP)$_2$(pmtH)] (pmtH is pyrimidine-2-thione) [33], {[AgCl(CMBZT)(TPTP)$_2$]·(MeOH)} (**1**) [17], [AgBr(TPP)(pmtH)]$_2$ [34] and [AgI(TPP)$_2$(MBZT)] [10]). In all complexes the intramolecular N–H···Cl hydrogen bonds additionally strengthen the tetrahedral coordination (Table 1 lists also the details of these interactions). The Ag–S bond distances in **2** and **3** are slightly longer than the corresponding bond distances reported for the terminal Ag–S bonds found in [AgCl(TPP)$_2$(MTZD)] [2.6629 (8) Å] [31], [AgCl(TPP)$_2$(pmtH)] [2.6151 (4) Å] [33], {[AgCl(CMBZT)(TPTP)$_2$]·(MeOH)} (**1**) [2.6486 (16) Å] [17], and [AgBr(TPP)(pmtH)]$_2$ [2.5548 (9) Å] [34] but they are similar in length to the ones found in [AgI(TPP)$_2$(MBZT)], where the Ag-S bond distances are 2.7825 (11) Å (molecule A) and 2.7159 (11) Å (molecule B) [10]. The variations in Ag–S bond distances observed among [AgCl(PR$_3$)(LS)] (PR$_3$ is triarylphospine, LS is thioamide) complexes might be attributed to the different electronic effects caused by the ligands.

In the case of **2** a neutral thioamide ligand MBZT is also cocrystallized in the unit cell, and it is also hydrogen-bonded with the chlorine atom. In this crystal structure the solvent (toluene) molecules occupy the empty spaces (Fig. 3b shows a fragment of the crystal packing after removal of the toluene molecules).

The calculated volumes of the Hirshfeld surfaces (Fig. 4) are 903.13 Å^3 (**1**), 1,391.51 Å^3 (**2**), and 998.18 Å^3 (**3**).

Table 1 Selected bond distances (Å), angles (°) and hydrogen bond data of $[AgCl(TPP)_2(MTZD)]$ (**1**), $\{[AgCl(TPP)_2(MBZT)]\cdot(MBZT)\cdot 2(toluene)\}$ (**2**), and $[AgCl(TPP)_2(CMBZT)]$ (**3**), where TPP is triphenylphosphine, MTZD is 2-mercaptothiazolidine, MBZT is 2-mercaptobenzothiazole, and CMBZT is 5-chloro-2-mercaptobenzothiazole

	1	2	3
Bond distances (Å)			
Ag1–Cl1	2.5596 (9)	2.6819 (11)	2.5585 (7)
Ag1–P2	2.4735 (8)	2.5106 (10)	2.4715 (7)
Ag1–P3	2.4832 (7)	2.4677 (9)	2.4704 (7)
Ag1–S42	2.6861 (10)	2.7037 (13)	2.7777 (8)
C42–S42	1.674 (4)	1.672 (5)	1.665 (3)
Bond angles (°)			
Cl1–Ag1–P2	112.53 (3)	105.61 (4)	113.14 (3)
Cl1–Ag1–P3	102.77 (3)	109.98 (3)	109.49 (3)
Cl1–Ag1–S42	102.68 (3)	104.91 (4)	101.65 (2)
P2–Ag1–P3	123.05 (3)	123.12 (3)	126.69 (2)
P2–Ag1–S42	110.25 (3)	99.90 (4)	93.63 (3)
P3–Ag1–S42	110.25 (3)	111.59 (4)	107.69 (3)
Hydrogen bonds			
H43···Cl1	2.17	2.24	2.19
N43···Cl1	3.082 (4)	3.102 (3)	3.046 (2)
N43–H43···Cl1	173	174	178

DNA binding studies

UV–vis spectroscopy

Absorption spectroscopy was used for the study of the binding properties of metal complexes with DNA [35]. Hyperchromism or hypochromism observed in the UV spectrum of the CT-DNA complex with respect to the corresponding spectrum of free CT-DNA is related to the configuration of the double helix structure of DNA [8]. The intercalative mode of binding usually results in hypochromism along with or without a small redshift or blueshift due to the strong stacking interaction between an aromatic chromophore and the base pairs of DNA [35].

The absorption spectra of **1–3** in the absence and presence of CT-DNA are shown in Fig. 5. The bands of **1–3** undergo hypochromism of about 22.3 % (**1**), 6.1 % (**2**), and 9.4 % (**3**). Moreover, in the case of **1**, a redshift of 5 nm is also observed, indicating that **1** binds to DNA through the conjugation of the aromatic rings with the stacking base pairs of the DNA helix [35]. In the case of complexes **2** and **3**, on the other hand, the simultaneous blueshifts of 2 and 1 nm, respectively, suggest binding through intercalation and electrostatic interaction of **2** and **3** with DNA bases [36].

To compare quantitatively the binding affinity of **1–3** towards CT-DNA, their binding constants (K_b) were determined [8] (Fig. 6, Table 2). The calculated K_b values for **1–3** are $(3.5 \pm 8.5) \times 10^4$, $(10.0 \pm 0) \times 10^4$, and $(46.4 \pm 7.0) \times 10^4\ M^{-1}$ respectively, confirming the interaction of **1–3** with CT-DNA (Table 2). Complexes **1–3** bind to CT-DNA in a manner similar to cisplatin

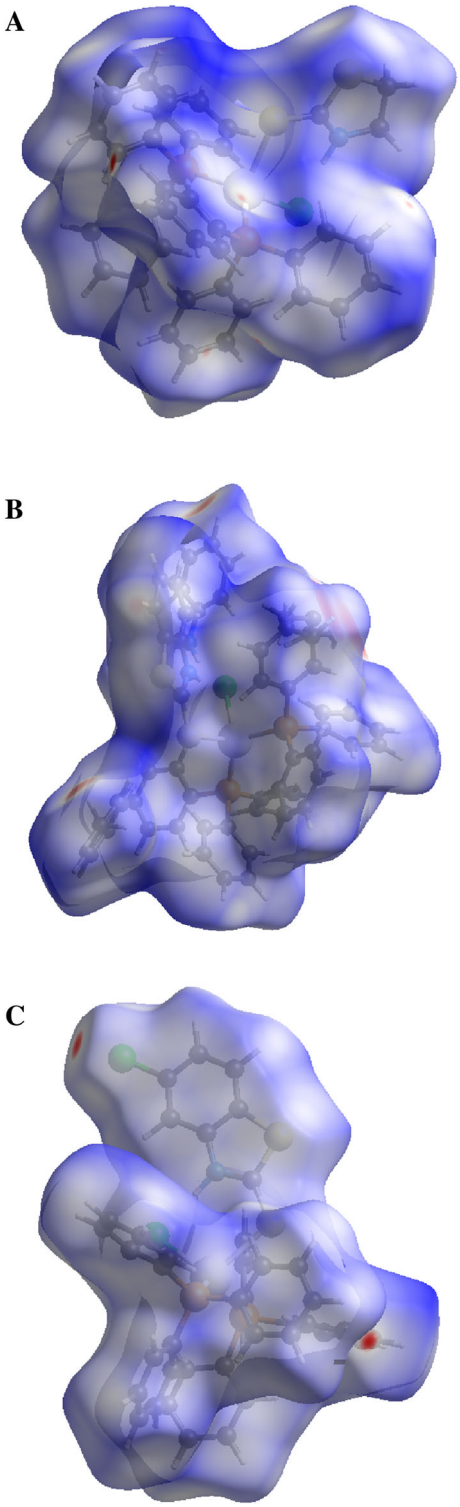

Fig. 4 Volumes of the Hirshfeld surfaces of **1** (**a**), **2** (**b**), and **3** (**c**)

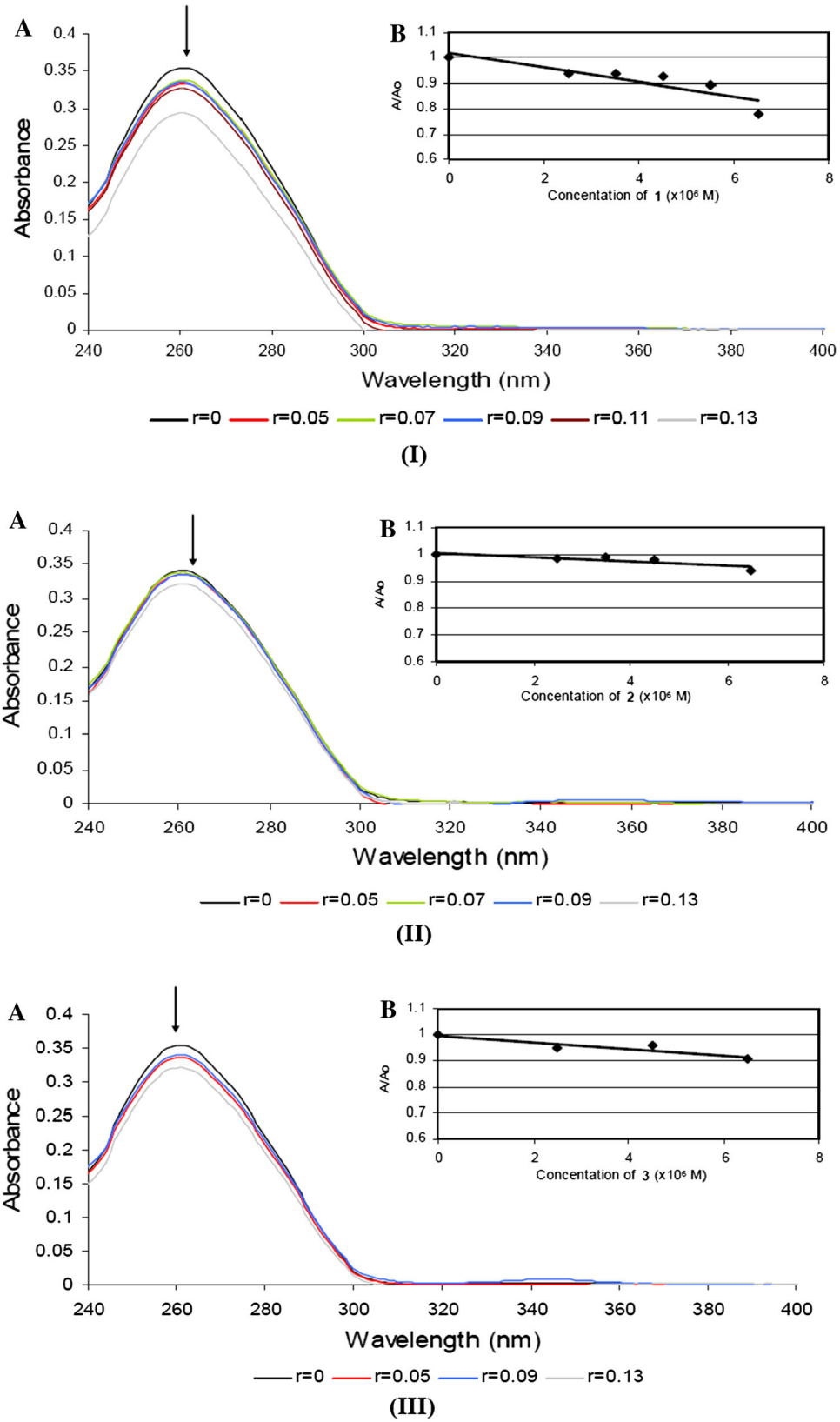

Fig. 5 UV spectra of calf-thymus DNA (CT-DNA) in buffer solution in the absence and presence of **1–3** at r values of 0, 0.05, 0.07, 0.09, 0.11, and 0.13 (r = [complex]/[DNA], 5×10^{-5} M DNA). The *insets* show A/A_o versus the concentration of the complex at λ_{max}

($K_b = (5.73 \pm 0.45) \times 10^4$ M^{-1} [8]). The binding affinity of **3** towards CT-DNA is highest among the mixed-ligand silver(I) complexes of triarylphosphine and anti-inflammatory drugs or thioamides tested by our group (Table 3). The K_b value of **3** is 1.5-fold higher than the corresponding value of {[$Ag(TPP)_3$(napr)](H_2O)} (naprH

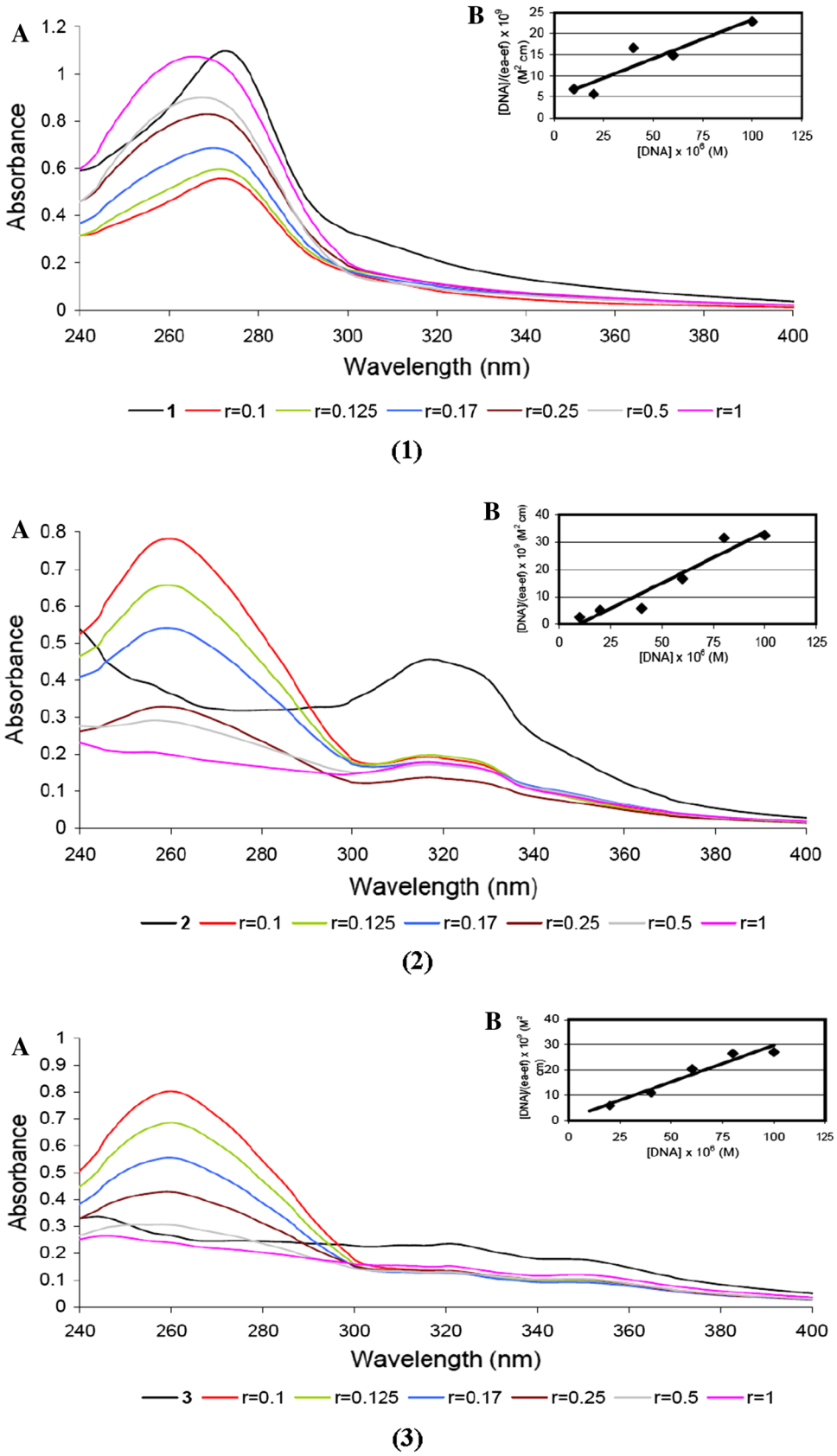

Fig. 6 UV spectra of complexes **1–3** in the absence and presence of CT-DNA at r values of 1, 0.5, 0.25, 0.17, 0.125, and 0.1 (r = [complex]/[DNA], 10 μM complex, 10–100 μM CT-DNA). The *insets* show [DNA]/($\varepsilon_\alpha - \varepsilon_f$) versus DNA concentration

Table 2 The DNA binding constants (K_b, K_{app}) of complexes **1–3**

Complex	Hypochromicity (%)	$\Delta\lambda$ (nm)	K_b ($\times 10^4$) (M^{-1})	K_{app} ($\times 10^4$) (M^{-1})
1	22.3	5	3.5 ± 0.7	1.1 ± 0.02
2	6.1	−2	10.0 ± 0	1.8 ± 0.44
3	9.4	−1	46.4 ± 7.0	2.2 ± 0.24

is naproxen, an anti-inflammatory drug) and is fourfold higher than that of {[Ag(TPP)$_3$(asp)](DMF)} (aspH is aspirin, an anti-inflammatory drug) [8, 9]. It is also twofold higher than the corresponding affinity of [Ag(TPP)$_2$(*p*-Hbza)], which contains *p*-hydroxybenzoic acid (*p*-HbzaH), a well-known antioxidant agent. The K_b value of [AgI(TPP)$_2$(MBZT)] [(10.7 ± 2.6) × 10^4 M^{-1}] (Table 3) [10] is in accordance with the corresponding value determined for **2**, which contains the same ligand. Thus, the kind of halogen which is coordinated to the silver ion (chlorine instead of iodine) exerts a minor influence on the binding properties of the complexes towards CT-DNA. Compound **2** also binds to DNA with K_b similar to that of [Ag(TPTP)$_2$(napr)] [(11 ± 2.8) × 10^4 M^{-1}] [9].

Fluorescence spectroscopy studies

Ethidium bromide (EtBr) is one of the most sensitive fluorescent probes that bind to DNA through intercalation [35]. The displacement of EtBr (quantified by fluorescence) by the titration of a compound is indicative of an intercalative or minor groove binding [37–42]. Competitive binding of drugs to DNA with EtBr could provide information with regard to the DNA binding affinity [35]. Two mechanisms have been proposed for the reduction in the emission intensity: the replacement of EtBr, and/or electron transfer [40]. Figure 7 shows the emission spectra at 610 nm of EtBr (2.3 μM) solutions containing CT-DNA (26 μM) in the absence or presence of various concentrations of complexes **1–3** (0–250 μM). The fluorescence quenching spectra illustrate that on increasing the concentration of the complexes **1–3**, the emission band at 610 nm exhibited hypochromism of 9.0, 16.4, and 19.1 %, respectively.

The apparent binding constant (K_{app}) was calculated using the equation [41]

$$K_{EtBr}[EtBr] = K_{app}[drug]_{50},$$

where $[drug]_{50}$ is the concentration of the complex causing a 50 % reduction of the fluorescence, $K_{EtBr} = 10^7$ M^{-1}, and [EtBr] = 2.3 μM [41]. The concentration of the drug causing a 50 % reduction of the fluorescence was calculated from the plot of I_0/I versus the concentration of the complex [Q] (Fig. 7), where I_0 and I are the fluorescence intensities of the CT-DNA in the absence and presence of complexes **1–3**, respectively. The linear Stern–Volmer equation is as follows:

$$I_0/I = 1 + K_{SV} \times [Q],$$

where K_{SV} is the Stern–Volmer dynamic quenching constant and [Q] is the total concentration of the quencher (complexes **1–3**) [37].

The K_{app} values calculated for complexes **1–3** are (3.5 ± 0.7) × 10^4 M^{-1} (**1**) (10.0 ± 0) × 10^4 M^{-1} (**2**), and (46.4 ± 7.0) × 10^4 M^{-1} (**3**) (Table 3), suggesting an intercalative or minor groove binding of the complexes. Complex **3** exhibits a high K_{app} value (Table 3). This might be due to the presence of the chlorine atoms which are involved in hydrogen-bonding interactions with the DNA bases. The mixed-ligand complex with naprH {[Ag(TPP)$_3$(napr)](H$_2$O)}, on the other hand, exhibits a higher K_{app} value than **3**, indicating its greater intercalative interaction with DNA or its better binding at the minor

Table 3 DNA binding constants (K_b, K_{app}) and half-maximal inhibitory concentrations (IC_{50}) towards lipoxygenase (*LOX*) caused by **1–3** and other related Ag(I) complexes

Complex	K_b ($\times 10^4$) (M^{-1})	K_{app} ($\times 10^4$) (M^{-1})	IC_{50} (μM) LOX	Reference
1	3.5 ± 0.7	1.1 ± 0.02	>30	This work
2	10.0 ± 0	1.8 ± 0.44	>30	This work
3	46.4 ± 7.0	2.2 ± 0.24	>30	This work
[AgI(TPP)$_2$(MBZT)]	10.7 ± 2.6	1.5 ± 0.1	>30	[10]
{[Ag(TPP)$_3$(napr)](H$_2$O)}	32.8 ± 8.5	2.9 ± 0.3	5.1	[9]
[Ag(TPTP)$_2$(napr)]	4.7 ± 1.8	1.6 ± 0.4	>30	[9]
{[Ag(TPP)$_3$(asp)](DMF)}	11 ± 2.8	–	7.2	[8]
[Ag(TPP)$_2$(salH)]	13.3 ± 6.5	–	2.3	[8]
[Ag(TPP)$_2$(*p*-Hbza)]	27.7 ± 7.9	–	7.6	[8]

aspH is aspirin, naprH is naproxen, and salH$_2$ is salicylic acid.

MBZT 2-mercaptobenzotiazole, *p-Hbza* p-hydroxybenzoic acid, *TPP* triphenylphosphine, *TPTP* tri(*p*-tolyl)phosphine

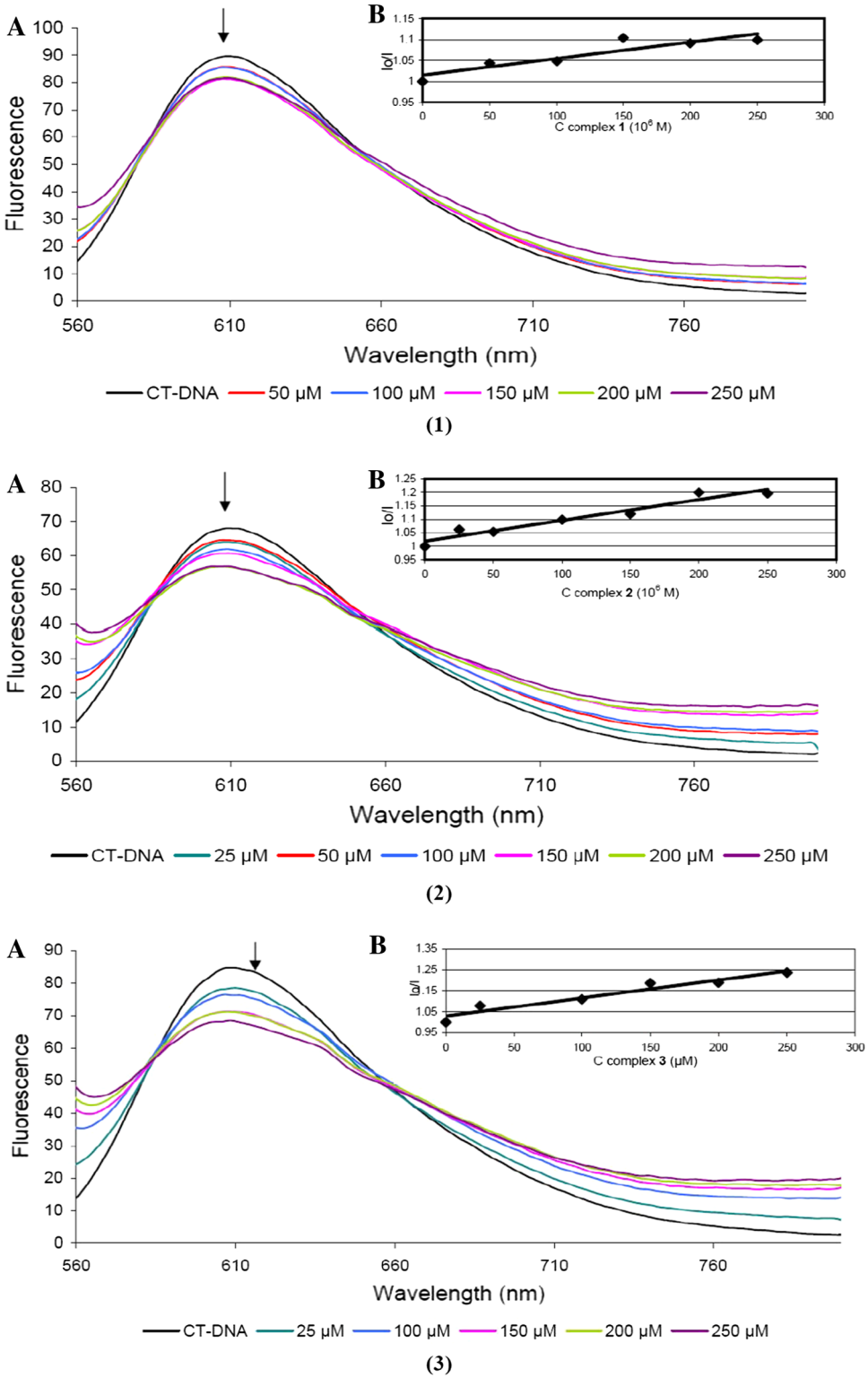

Fig. 7 Emission spectra of ethidium bromide bound to DNA in the presence of **1**–**3** (2.3 μM ethidium bromide, 26 μM DNA, 0–250 μM complex, $\lambda_{ex} = 527$ nm). The *arrow* shows the intensity changing on increasing the concentration of complexes **1**–**3**. The *insets* shows I_0/I versus the concentration of the complex

groove. It is known that compounds which inhibit malignant cells interact with DNA [42], and small DNA binders interact with DNA either by intercalating in between the base pairs or by docking in the minor groove, or both. Therefore, **3** may be an efficient new small DNA binder.

Inhibitory activity of **1**–**3** towards the peroxidation of linoleic acid by the enzyme LOX

LOX inhibition is known to induce apoptosis [8, 43, 44]. The influence of complexes **1**–**3** on the oxidation of linoleic

acid by the enzyme LOX was studied over a wide concentration range. The degree of LOX activity in the presence of **1–3** was calculated according to the method described previously [8]. Figure 8 shows LOX activity versus various concentrations of complexes **1–3**. All three complexes show no inhibitory activity towards LOX, and we were unable to determined the half-maximal inhibitory concentrations (IC_{50}) within the concentrations used (0–30 μM) ($IC_{50} > 30$ μM) (Fig. 8, Table 3). This is in agreement with the results obtained for $[AgI(TPP)_2(MBZT)]$, where also no inhibitory activity was detected [10]. Thus, **1–3** may act through interaction with DNA rather than interfering with LOX. Moreover, although mixed-ligand silver(I) complexes of anti-inflammatory drugs as ligands (aspH, naprH, or $salH_2$) and triarylphosphines inhibit LOX activity in very low concentrations ($[Ag(TPP)_2(salH)]$, $IC_{50} = 2.3$ μM;, $\{[Ag(TPP)_3(napr)](H_2O)\}$, $IC_{50} = 5.1$ μM); $\{[Ag(TPP)_3(asp)](DMF)\}$, $IC_{50} = 7.2$ μM) (Table 3), the mixed-ligand silver(I) complexes of thioamides and triarylphosphines exhibit no such activity. Therefore, the anti-inflammatory drugs affect the LOX inhibitory activity.

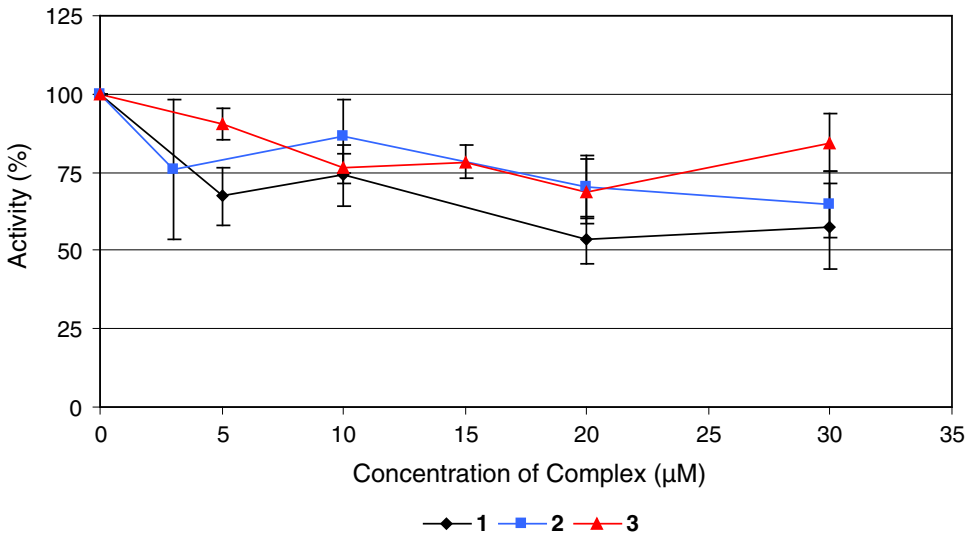

Fig. 8 Lipoxygenase activity versus various concentrations of complexes **1–3**

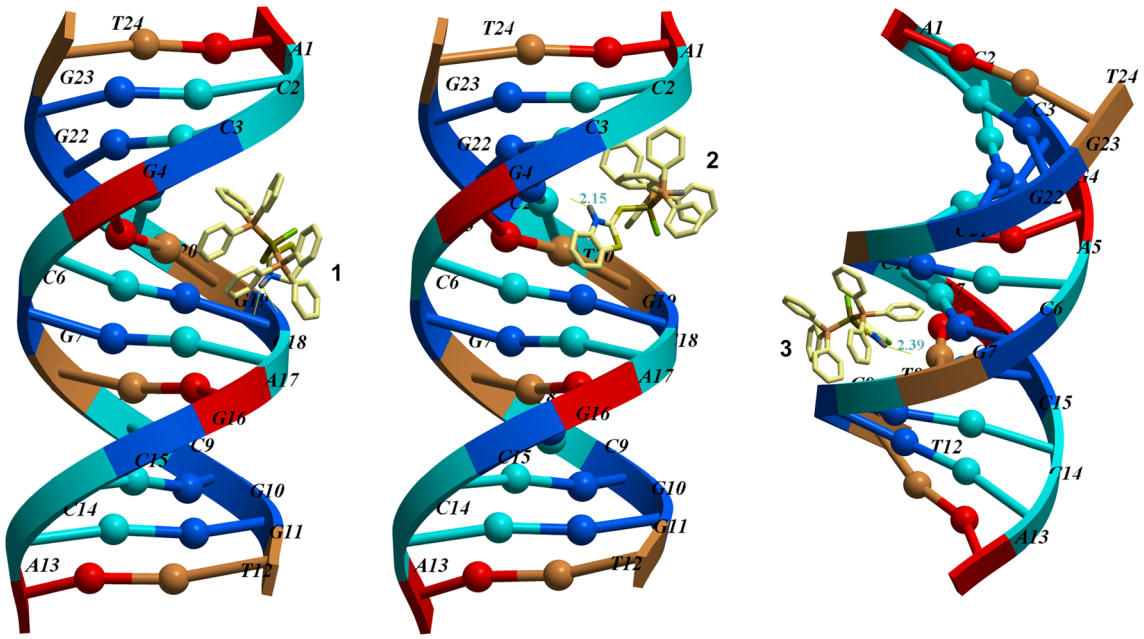

Fig. 9 Binding sites and hydrogen-bonding interactions of **1–3** towards CT-DNA

Computational studies

DNA docking

Knowledge of how cisplatin inhibits DNA replication and transcription has led to a dramatic increase in the number of new metal complexes as promising metallotherapeutics [45]. DNA docking studies were performed for all three complexes with regard to CT-DNA. The lowest-energy conformations show that **1** and **2** bind to the major groove near the domain of guanines G19 and G4 (Fig. 9). Complex **1** forms two hydrogen bonds with O2 and O5 of G19 at 2.52 and 2.69 Å with the protonated nitrogen atom, and **2** form a hydrogen bond with the O6 atom of G4 at 2.15 Å. The conformation energies were calculated to be −87.89 and −77.95 kcal mol^{-1} for **1** and **2**, respectively. In contrast, **3** prefers the minor groove, where, in general, the electronegative AT sequences are closer and exhibit shorter van der Waals contacts compared with the GC regions. This result is in agreement with the experimentally found high K_{app} value (Table 2), where significant steric interactions and better binding affinity were found. Complex **3** exhibits hydrogen bonding between the N^+ atom of the ligand and the O2 atom of thymine T8 at 2.39 Å. No hydrogen-bonding interactions were revealed for the chlorine atoms of the ligand, although they cannot be excluded for conformations with similar orientation and energy. The latter was calculated to be −99.95 kcal mol^{-1}.

LOX docking

Blocking LOX is strongly related to tumor cell proliferation and apoptosis in several tumor cell types [46]. The binding affinity of complexes **1–3** was explored by molecular docking methods to evaluate their potential inhibitory effectiveness.

All complexes dock away from the central iron atom, which was identified as the active site of the enzyme [47], and owing to their large dimensions they prefer surface cavities to exert their binding activity. Furthermore, they cannot reach the largest pocket (green sphere in Fig. 10), which has been suggested as a possible site associated with an enhanced inhibitory effect [22, 23] in agreement with the experimental results where no inhibitory activity towards LOX was found for the complexes studied.

The results showed that **1** resides in the cavity/surface formed by Ala540, Arg242, Asn245, Asn537, Gln544, Glu106, Glu179, Glu236, Glu256, Ile257, Leu541, Lys17, Lys260, Met536, Phe238, Pro241, Tyr132, Tyr239, Val237, and Val240 at an Ag–Fe distance of 18.8 Å. Complexes **2** and **3** share similar behavior and a similar docking site with the common residues Ala569, Arg360, Arg588, Asn370, Asn573, Asp408, Asp411, Cys357, Ile412, Leu501, Lys587, Trp574, Tyr493, Tyr571, Val358, Val570, and Val575. Significant steric interactions as revealed by pairwise linear potential calculations are evident with Arg360, Asn573, Ile412, Tyr493, and Val570.

Effects of complexes **1–3** on the growth of microbial strains

The noteworthy high binding affinity of **1–3** towards CT-DNA led us to evaluate their antibacterial activity. It is well known that the antibacterial action of silver compounds appears to involve interaction with DNA [1, 2]. To test the possible effects of silver complexes on the growth of

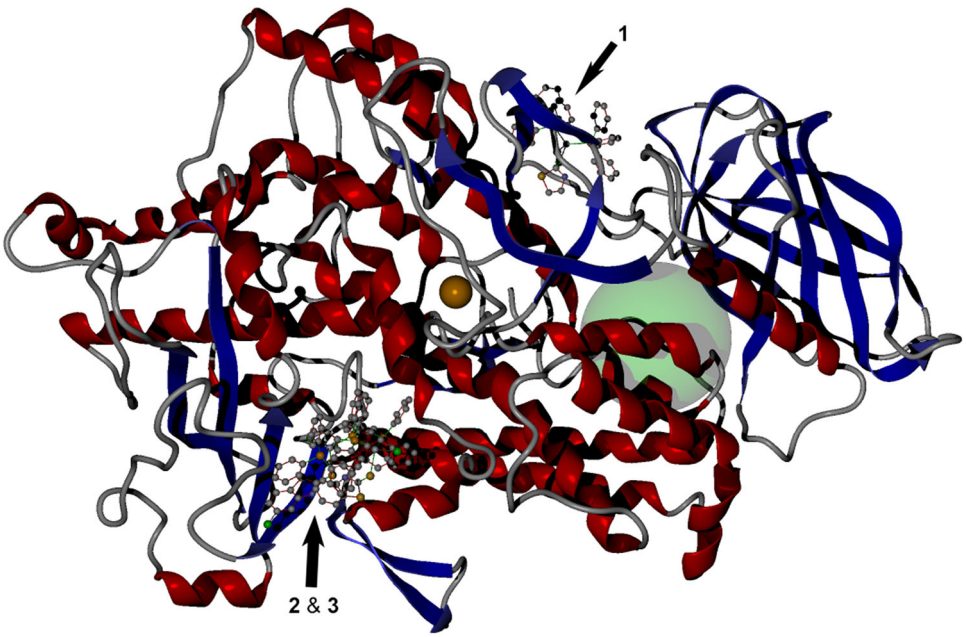

Fig. 10 Binding sites for complexes **1–3** with regard to lipoxygenase

microbial cells, two microbial species were used: *P. aeruginosa* and *E. coli*. The minimum inhibitory concentration (MIC) of **1** that prevents growth overnight of *P. aeruginosa* bacteria was found to be 150 μM, whereas the corresponding MIC of silver nitrate was 60 μM. The MICs of **2** and **3** with regard to *P. aeruginosa* are higher than 400 μM. The MICs of **2** and **3** could not be determined since the effect of DMSO, which was used as a solvent for the stock solutions of the complexes (final DMSO concentration 4 % v/v), is detrimental to cell growth for high concentrations of the complexes. The MICs of **1–3** with regard to *E. coli* cells show higher activity of **1** [40 μM for **1**, more than 400 μM for **2**, and 300 μM for **3**); the MIC of silver nitrate is 25 μM. The effect of DMSO on cell growth was visible again above 4 % v/v. The significantly high activity of **1** against both microbial strains is in agreement with its ability to bind DNA (see earlier). The negligible activity, however, observed in the case of **2** and **3** might be due to either variable resistance of the bacterial strains to these complexes compared with complex **1** [48] or differences in basal uptake rates and efflux rates for complexes **2** and **3** in comparison with complex **1**. The higher MICs of silver complexes with regard to *P. aeruginosa* compared with *E. coli* could be assigned to the lower outer membrane permeability. This hypothesis is strengthened by the fact that although the multidrug and toxic compound extrusion gene families are similar in both *E. coli* and *P. aeruginosa*, the *P. aeruginosa* genome contains many more predicted multidrug efflux systems [49]. Moreover, *P. aeruginosa* is well known for its intrinsic resistance to many front-line antibiotics, due mainly to its low outer membrane permeability and to active efflux [50].

Despite the high activity found for silver nitrate against both microbial strains, the main problem with the use of this salt in medicine is its high solubility in water, with its simultaneous very low lipophilicity. Thus, the silver ions immediately released after silver nitrate application are chemically consumed and rapidly inactivated through the formation of chemical complexes by chloride within a few hours [4]. Complex **1** overcomes this problem since it has been designed to be stable and to be soluble in organic media.

Conclusions

Three silver(I) chloride complexes—**1–3**—were synthesized and fully characterized. The geometry around the metal center in **1–3** is tetrahedral. Complexes **1–3** exhibit photosensitivity on UV radiation, whereas they are stable during biological experiments. Triphenylphosphine oxide was detected in the irradiated solution, suggesting photodecomposition of the initial compounds on radiation with UV-C light.

The binding constants (K_b) of **1–3** towards CT-DNA calculated from the UV–vis spectra (Table 3) indicate that **2** and **3** bind strongly to DNA, whereas **1** exhibits lower affinity for DNA. Thus, the kind of the thioamide ligand affects the binding properties. Among **2** and **3**, the latter exhibits 4.5-fold higher activity (Table 3), which might be attributed to the chlorine substituent of the CMBZT ligand and its interaction with DNA bases. The K_b value of $[AgI(TPP)_2(MBZT)]$ (Table 3) [10] is similar to the corresponding value determined for **2**, which contains the same ligand. Thus, the kind of halogen which is coordinated to the silver ion (chlorine instead of iodine) exerts a minor influence on the binding properties of the complexes towards CT-DNA. The corresponding apparent binding constants (K_{app}) towards CT-DNA were calculated from the changes in fluorescence of EtBr. Complex **3** exhibits a high K_{app} value (Table 3). The mixed-ligand complex with naprH $\{[Ag(tpp)_3(napr)](H_2O)\}$, on the other hand, exhibits a higher K_{app} value than **3**, indicating its greater intercalative interaction with DNA or its better binding at the minor groove. The low theoretical binding energy of **1–3** with regard to CT-DNA reveals that **1** and **2** biud to the major groove, and **3** binds to the minor groove. This is in agreement with the higher K_{app} value (Table 3) measured experimentally for **3**.

The inhibitory activity of **1–3** towards LOX is negligible at concentrations of 1–30 μM. This is in accordance with the inhibitory activity found for $[AgI(TPP)_2(MBZT)]$, which also exhibits no inhibitory activity at the same concentrations. In contrast, mixed-ligand silver(I) complexes of anti-inflammatory drugs as ligands (aspH, naprH, or $salH_2$) and triarylphosphines inhibit LOX activity at very low concentrations (Table 3). Therefore, the presence of halogen atoms and thioamides in the coordination sphere of the silver(I) ion eliminates the LOX inhibitory activity of the complexes, and the anti-inflammatory drugs in the complexes enhance their LOX inhibitory activity. Molecular docking studies have shown that **1–3** dock far away from the iron atom, which was identified as the active site of the enzyme [27], and even further from the larger pocket, which possibly acts as an allosteric site [22] (Fig. 10). This orientation of **1–3**, far away from the active or allosteric sites of LOX, might explain their negligible inhibitory activity found experimentally (see earlier).

Complex **1** was found to inhibit both the *P. aeruginosa* and *E. coli*, whereas **2** and **3** exhibit negligible activity. This might be due to either the variable resistance of the bacterial species against these complexes compared with complex **1** [48] or differences in basal uptake rates and efflux rates for **2** and **3** in comparison with **1**. This is further supported by the lower volumes of the Hirshfeld surface

calculated for **1** in contrast to **2** and **3**. It is also concluded that the antibacterial activity of **1**–**3** against *E. coli* is in the same order as the volumes of the Hirshfeld surfaces.

Materials and methods

Materials and instruments

All solvents used were of reagent grade. Silver(I) chloride was prepared by mixing aqueous solutions of $AgNO_3$ (Degussa) with an appropriate amount of NaCl (Aldrich). The precipitates were filtered off and dried in darkness. TPP and the thioamides MTZD, MBZT, and CMBZT (Merck) were used with no further purification. DMSO and boric acid were from Riedel-de Haën. Melting points were measured in open tubes with a Stuart Scientific apparatus and are uncorrected. IR spectra in the region from 370 to 4,000 cm^{-1} were obtained from KBr discs, with a PerkinElmer Spectrum GX Fourier transform IR spectrophotometer. The ^{1}H-NMR spectra were recorded with a Bruker AC 250-MHz Fourier transform NMR instrument in DMSO-d_6 solution. A JASCO UV–vis/near IR V570 series spectrophotometer was used to obtain electronic absorption spectra. Fluorescence spectra were recorded with a PerkinElmer LS55 fluorimeter Conductivity measurements were conducted at 20 °C in DMSO solutions with a WTF LF-91 conductivity meter.

Synthesis and crystallization of **1**–**3**

Complexes **1**–**3** were synthesized as follows.

A toluene suspension (20 ml) containing 0.5 mmol AgCl (0.072 g), 1 mmol TPP (0.262 g), and 0.5 mmol of the appropriate thioamide—MTZD (0.059 g) (**1**), MBZT (0.167 g) (**2**), or CMBZT (0.101 g) (**3**)—was heated under reflux for 2 h. The clear solutions were filtered and the filtrates were kept in darkness. After a few days, white crystals (**1**), yellow crystals (**2**), and pale-yellow crystals (**3**) suitable for X-ray crystallographic analysis were precipitated.

Complex **1**. Yield 62%, molar mass 787 g/mol, melting point 202–209 °C. IR (cm^{-1}) (KBr): 3,450 (m), 3,137 (m), 2,932 (m), 1,709 (w), 1,518 (w), 1,478 (s), 1,433 (s), 1,093 (m), 748 (s), 696 (vs), 508 (m), 486 (m). Solubility: acetone, acetonitrile, toluene, DMF, DMSO, methanol, ethanol.

Complex **2**. Yield 56 %, molar mass 1,172 g/mol, melting point 134–138 °C. IR (cm^{-1}) (KBr): 3,449 (m), 3,001 (m), 2,944 (m), 1,897 (w), 1,585 (m), 1,493 (m), 1,431 (s), 1,094 (s), 744 (s), 695 (s), 513 (s), 439 (s). Solubility: acetone, acetonitrile, toluene, DMF, DMSO, methanol, ethanol.

Complex **3**. Yield 69 %, molar mass 869 g/mol, melting point 189–194 °C. IR (cm^{-1}) (KBr): 3,449 (m), 3,064 (m), 2,622 (m), 1,655 (m), 1,586 (m), 1,478 (s), 1,434 (vs), 1,313 (s), 1,080 (vs), 744 (vs), 689 (vs), 502 (vs). Solubility: acetone, acetonitrile, toluene, chloroform, DMF, DMSO.

X-ray structure determination

Diffraction data for the complexes were collected at room temperature by ω scan with a SuperNova diffractometer (Atlas detector) with mirror-monochromatized Cu Kα radiation ($\lambda = 1.54178$ Å) for **1** and **2** and with an Xcalibur diffractometer (Eos detector) with graphite-monochromatized Mo Kα radiation ($\lambda = 0.71073$ Å) for **3**. The data were corrected for Lorentz-polarization and absorption effects [51]. Accurate unit-cell parameters were determined by a least-squares fit of the reflections of the highest intensity, chosen from the whole experiment. The structures were solved with SIR92 [52] and were refined with the full-matrix least-squares procedure on F^2 by SHELXL-2013 [53]; most of the calculations were performed within the WinGX program suite [54]. Scattering factors incorporated in SHELXL-2013 were used. All non-hydrogen atoms were refined anisotropically; hydrogen atoms were placed in the calculated positions, and were refined as a "riding model" with the isotropic displacement parameters set at 1.2 times (1.5 times for methyl groups) the U_{eq} value for appropriate non-hydrogen atoms. In the crystal structure of **2**, the voids are occupied by partially disordered solvent (toluene) molecules; the geometry and displacement parameters for the solvent molecules were restrained. The Alert A in the checkcif of **2** is connected with the heavily disordered part of the structure; this short contact is the result of this disorder. Relevant crystal data are listed in Table 4, together with refinement details.

The volumes of the Hirshfeld surface [55] were calculated with the program CrystalExplorer [56].

Crystallographic data (excluding structure factors) for the structural analysis have been deposited with the Cambridge Crystallographic Data Centre (CCDC), nos. CCDC-956172 (**1**), CCDC-956173 (**2**), and CCDC-956174 (**3**). Copies of this information may be obtained free of charge from the CCDC (The Director, CCDC, 12 Union Road, Cambridge, CB2 1EZ, UK; Fax: +44-1223-336033; e-mail: deposit@ccdc.cam.ac.uk; website: http://www.ccdc.cam.ac.uk).

Biological tests

DNA binding studies

This study was conducted as reported in [8].

Table 4 Crystal data, data collection, and structure refinement

	1	**2**	**3**
Formula	$C_{39}H_{35}AgClNP_2S_2$	$C_{43}H_{35}$ $AgClNP_2S_2{\cdot}C_7H_5NS_2{\cdot}1.5(C_7H_8)$	$C_{43}H_{34}$ $AgCl_2NP_2S_2$
Formula weight	787.06	1,140.54	869.54
Crystal system	Monoclinic	Triclinic	Monoclinic
Space group	$P2_1/c$	P-1	$P2_1/c$
a (Å)	14.1445 (8)	13.0484 (5)	14.8878 (3)
b (Å)	10.3249 (6)	13.5500 (5)	10.2774 (3)
c (Å)	25.1116 (17)	17.4727 (10)	26.4302 (8)
α (°)	90	70.489 (4)	90
β (°)	94.643 (6)	76.483 (4)	92.702 (3)
γ (°)	90	78.754 (3)	90
V (Å^3)	3,655.3 (4)	2,808.1 (2)	4,039.5 (2)
Z	4	2	4
d_x (g cm^{-3})	1.43	1.35	1.43
F(000)	1,608	1,174	1,768
μ (mm^{-1})	7.21	5.55	0.85
Θ range (°)	3.14–75.61	3.49–70.00	1.37–26.52
hkl range	$-17 \leq h \leq 17$	$-15 \leq h \leq 15$	$-18 \leq h \leq 18$
	$-12 \leq k \leq 12$	$-16 \leq h \leq 15$	$-12 \leq h \leq 10$
	$-31 \leq l \leq 26$	$-20 \leq h \leq 21$	$-31 \leq h \leq 32$
Reflections			
Collected	21,054	23,837	17,729
Unique (R_{int})	7,395 (0.036)	10,616 (0.038)	8,166 (0.026)
With $I > 2\sigma$ (I)	6,791	7,763	7,236
Number of parameters	419	622	460
R (F) [$I > 2\sigma$ (I)]	0.046	0.053	0.038
wR (F^2) [$I > 2\sigma$ (I)]	0.125	0.147	0.108
R (F) (all data)	0.050	0.071	0.043
wR (F^2) (all data)	0.129	0.158	0.113
Goodness of fit	1.05	1.00	0.80
Max/min $\Delta\rho$ (e^- Å^{-3})	1.31/−1.06	0.84/−0.65	0.87/−0.67

Fluorescence spectroscopy studies

The fluorescence spectroscopy method using EtBr was used to determine the relative DNA binding properties of complexes **1–3** with regard to CT-DNA. The emission spectra at 610 nm of EtBr (2.3 μM) solutions containing CT-DNA (26 μM) in the absence or presence of various concentrations of complexes **1–3** (0, 25, 50, 100, 150, 200, and 250 μM) were recorded on their excitation at 527 nm [9, 10, 57].

Study of the peroxidation of linoleic acid by the enzyme LOX in the presence of complexes

This study was performed as reported in [8].

Computational details

Molecular docking studies were performed for LOX (Protein Data Bank ID 1F8N) similarly to the procedure described in [23]. DNA docking was conducted according to [8].

Bacterial cultures and estimation of MIC

P. aeruginosa PAO1 and *E. coli* Mach1 (Invitrogen) bacterial strains were grown overnight in Luria–Bertani (LB) broth with vigorous shaking at 37 °C. After 1 day, LB agar plates supplemented with serial concentrations of **1–3**, silver nitrate, and DMSO were poured and immediately inoculated with the appropriate inoculum of either

P. aeruginosa PAO1 or *E. coli* overnight cultures. Plates were incubated for 24 h at 37 °C. The MIC was defined as the lowest concentration of the supplements that inhibits visible bacterial growth after overnight incubation. In all cases, LB plates without any supplement were also inoculated (controls). The experiment was performed with three biological replicates.

Acknowledgments This work was conducted in partial fulfillment of the requirements for the graduate studies of L.K. (PhD) and C.N.B. (master) under the supervision of S.K.H within the framework of the graduate program in bioinorganic chemistry. The National Strategic Reference Framework, Regional Operational Program of Epirus 2007-2013 (2011/S 29-048013), is acknowledged for supporting the purchase of an LS55 fluorimeter by the Department of Chemistry of the University of Ioannina. A. Koukou (Department of Chemistry, University of Ioannina) is acknowledged for the supply of *P. aeruginosa* PAO1 cells.

References

1. Klasen HJ (2000) Burns 26:117–130
2. Silver S, Phung LT, Silver G (2006) Ind Microbiol Biotechnol 33:627–634
3. Melaiye A, Youngs W (2005) Expert Opin Ther Pat 15:125–130
4. Klasen HJ (2000) Burns 26:131–138
5. Feng QL, Wu J, Chen GQ, Cui FZ, Kim TN, Kim JOJ (2000) Biomed Mater Res 52:662–668
6. Modak SM, Fox CL Jr (1973) Biochem Pharmacol 22:2391–2404
7. Banti CN, Hadjikakou SK (2013) Metallomics 5:569–596
8. Banti CN, Giannoulis AD, Kourkoumelis N, Owczarzak A, Poyraz M, Kubicki M, Charalabopoulos K, Hadjikakou SK (2012) Metallomics 4:545–560
9. Banti CN, Giannoulis AD, Kourkoumelis N, Owczarzak AM, Kubicki M, Hadjikakou SK (2013, in press)
10. Banti CN, Kyros L, Geromichalos GD, Kourkoumelis N, Kubicki M, Hadjikakou SK (2013, in press)
11. Samuelsson B, Dahlen SE, Lindgren J, Rouzer CA, Serhan CN (1987) Science 237:1171–1176
12. Knapp MJ, Klinman JP (2003) Biochemistry 42:11466–11475
13. Zha S, Yegnasubramanian V, Nelson WG, Isaacs WB, De Marzo AM (2004) Cancer Lett 215:1–20
14. Tong WG, Ding XZ, Witt RC, Adrian TE (2002) Mol Cancer Ther 1:929–935
15. Hansen J, Garreta A, Benincasa M, Carmen Fusté M, Busquets M, Manresa A (2013) Appl Microbiol Biotechnol 97:4737–4747
16. Poyraz M, Banti CN, Kourkoumelis N, Dokorou V, Manos MJ, Simčič M, Golič-Grdadolnik S, Mavromoustakos T, Giannoulis AD, Verginadis II, Charalabopoulos K, Hadjikakou SK (2011) Inorg Chim Acta 373:114–121
17. Kyros L, Kourkoumelis N, Kubicki M, Male L, Hursthouse M, Verginadis II, Gouma E, Karkabounas S, Charalabopoulos K, Hadjikakou SK (2010) Bioinorg Chem Appl. doi:10.1155/2010/386860
18. Zartilas S, Hadjikakou SK, Hadjiliadis N, Kourkoumelis N, Kyros L, Kubicki M, Baril M, Butler IS, Karkabounas S, Balzarini J (2009) Inorg Chim Acta 362:1003–1010
19. Zachariadis PC, Hadjikakou SK, Hadjiliadis N, Skoulika S, Michaelides A, Balzarini J, De Clercq E (2004) Eur J Inorg Chem 2004:1420–1426
20. Ozturk II, Banti CN, Manos MJ, Tasiopoulos AJ, Kourkoumelis N, Charalabopoulos K, Hadjikakou SK (2012) J Inorg Biochem 109:57–65
21. Ozturk II, Urgut OS, Banti CN, Kourkoumelis N, Owczarzak AM, Kubicki M, Charalabopoulos K, Hadjikakou SK (2013) Polyhedron 52:1403–1410
22. Ozturk I, Filimonova S, Hadjikakou SK, Kourkoumelis N, Dokorou V, Manos MJ, Tasiopoulos AJ, Barsan MM, Butler IS, Milaeva ER, Balzarini J, Hadjiliadis N (2010) Inorg Chem 49:488–501
23. Balas VI, Banti CN, Kourkoumelis N, Hadjikakou SK, Geromichalos GD, Sahpazidou D, Male L, Hursthouse MB, Bednarz B, Kubicki M, Charalabopoulos K, Hadjiliadis N (2012) Aust J Chem 65:1625–1637
24. Balas VI, Verginadis II, Geromichalos GD, Kourkoumelis N, Male L, Hursthouse MB, Repana KH, Yiannaki E, Charalabopoulos K, Bakas T, Hadjikakou SK (2011) Eur J Med Chem 46:2835–2844
25. Xanthopoulou MN, Hadjikakou SK, Hadjiliadis N, Schurmann M, Jurkschat K, Michaelides A, Skoulika S, Bakas T, Binolis J (2003) J Inorg Biochem 96:425–434
26. Abdellah MA, Hadjikakou SK, Hadjiliadis N, Kubicki M, Bakas T, Kourkoumelis N, Simos YV, Karkabounas S, Barsan M, Butler IS (2009) Bioinorg Chem Appl. doi:10.1155/2009/542979
27. Xanthopoulou MN, Hadjikakou SK, Hadjiliadis N, Milaeva ER, Gracheva JA, Tyurin VY, Kourkoumelis N, Christoforidis KC, Metsios AK, Karkabounas S, Charalabopoulos K (2008) Eur J Med Chem 43:327–335
28. Kouroulis KN, Hadjikakou SK, Kourkoumelis N, Kubicki M, Male L, Hursthouse M, Skoulika S, Metsios AK, Tyurin VY, Dolganov AV, Milaeva ER, Hadjiliadis N (2009) Dalton Trans 10446–10456
29. Lazarou K, Bednarz B, Kubicki M, Verginadis II, Charalabopoulos K, Kourkoumelis N, Hadjikakou SK (2010) Inorg Chim Acta 363:763–772
30. Velalopoulou A, Batsala GK, Kourkoumelis N, Karkabounas S, Evangelou A, Hadjikakou SK (2013) Med Chem Res 22:2260–2265
31. Sultana R, Lobana TS, Sharma R, Castineiras A, Akitsu T, Yahagi K, Aritake Y (2010) Inorg Chim Acta 363:3432
32. Hilliard HM, Yoke JT (1966) Inorg Chem 5:57–61
33. Batsala GK, Dokorou V, Kourkoumelis N, Manos MJ, Tasiopoulos AJ, Mavromoustakos T, Simčič M, Golič-Grdadolnik S, Hadjikakou SK (2013) Inorg Chim Acta 382:146–157
34. Cox PJ, Aslanidis P, Karagiannidis P, Hadjikakou SK (2000) Inorg Chim Acta 310:268–272
35. Alagesan M, Bhuvanesh NSP, Dharmaraj N (2013) Dalton Trans 42:7210–7223
36. Zhang G, Hu X, Zhao N, Li W, He L (2010) Pest Biochem Physiol 98:206–212
37. Anbu S, Kandaswamy M, Kamalraj S, Muthumarry J, Varghese B (2011) Dalton Trans 40:7310–7319
38. Afrati T, Pantazaki AA, Dendrinou-Samara C, Raptopoulou C, Terzis A, Kessissoglou DP (2010) Dalton Trans 39:765–775
39. Palchaudhuri R, Hergenrother PJ (2007) Curr Opin Biotechnol 18:497–503
40. Dimiza F, Papadopoulos AN, Tangoulis V, Psycharis V, Raptopoulou CP, Kessissoglou DP, Psomas G (2010) Dalton Trans 39:4517–4528
41. Lee M, Rhodes AL, Wyatt MD, Forrow S, Hartley JA (1993) Biochemistry 32:4237–4245
42. Barawkar DA, Ganesh KN (1995) Nucleic Acids Res 23:159–164
43. Ding XZ, Kuszynski CA, El-Metwally TH, Adrian TE (1999) Biochem Biophys Res Commun 266:392–399
44. Husson F, Pagot Y, Kermasha S, Belin JM (1998) Enzyme Microb Technol 23:42–48
45. Zhang CX, Lippard SJ (2003) Curr Opin Chem Biol 7:481–489
46. Tong WG, Ding XZ, Adrian TE (2002) Biochem Biophys Res Commun 296:942–948
47. Minor W, Steczko J, Stec B, Otwinowski Z, Bolin JT, Walter R, Axelrod B (1996) Biochemistry 35:10687–10701

48. Chopra I (2007) J Antimicrob Chemother 59:587–590
49. Stover CK, Pham XQ, Erwin AL, Mizoguchi SD, Warrener P, Hickey MJ, Brinkman FSL, Hufnagle WO, Kowalik DJ, Lagrou M, Garber RL, Goltry L, Tolentino E, Westbrock-Wadman S, Yuan Y, Brody LL, Coulter SN, Folger KR, Kas A, Larbig K, Lim R, Smith K, Spencer D, Wong GK-S, Wu Z, Paulsen IT, Reizer J, Saier MH, Hancock REW, Lory S, Olson MV (2000) Nature 406:959–964
50. Hancock RE (1998) Clin Infect Dis 27:93–99
51. Agilent Technologies (2012) CrysAlis^{Pro}. Agilent Technologies, Santa Clara
52. Altomare A, Cascarano G, Giacovazzo C, Guagliardi A, Burla MC, Polidori G, Camalli M (1994) J Appl Crystallogr 27:435
53. Sheldrick GM (2008) Acta Crystallogr Sect A 64:112–122
54. Farrugia LJ (2012) J Appl Crystallogr 45:849–854
55. Spackman MA, Jayatilaka D (2009) CrystEngComm 11:19–32
56. Wolff SK, Grimwood DJ, McKinnon JJ, Turner MJ, Jayatilaka D, Spackman MA (2012) CrystalExplorer, version 3.0. University of Western Australia, Crawley
57. Zhao Y, Zhu J, He W, Yang Z, Zhu Y, Li Y, Zhang J, Guo Z (2006) Chem Eur J 12:6621